euspen's 21st International Conference & Exhibition, Copenhagen, DK, June 2021
www.euspen.eu

# Experimental characterisation of performances of optimized piezoelectric energy harvesters

Petar Gljušćić,[1, 2] Saša Zelenika,[1, 2, 3] Marko Perčić [1, 2, 3] and Ervin Kamenar [1, 2, 3]

[1] *University of Rijeka, Faculty of Engineering, Precision Engineering Laboratory, Vukovarska 58, 51000 Rijeka, CROATIA*
[2] *University of Rijeka, Centre for Micro- and Nanosciences and Technologies, Laboratory for Precision Engineering and the Micro- and Nanosystems Technologies, Radmile Matejčić 2, 51000 Rijeka, CROATIA*
[3] *University of Rijeka, Centre for Artificial Intelligence and Cybersecurity, Laboratory for AI in Mechatronics, Radmile Matejčić 2, 51000 Rijeka, CROATIA*

sasa.zelenika@riteh.hr

**Abstract**
The growing use of energy harvesting in wearable technologies made evident the potential limits in applying piezoelectric devices excited by random human motion. Piezoelectric energy harvesters are, in fact, characterised by a narrow area of optimal operation around their eigenfrequency. An optimization of the design parameters of such harvesters by using the design-of-experiments methodology, coupled with suitable frequency up-conversion excitation, can lead to the development of improved configurations of functional wearable devices. The validation of this approach via elaborated finite element models performed in this work allows proving its validity, but the resulting designs have to be experimentally verified as well. Suitable experimental setups, enabling harmonic, as well as frequency up-conversion excitation, are thus developed, enabling the validation of different dynamical conditions. The thus obtained experimental responses are compared to those attained via numerical simulations, allowing to deduce considerations important for the development of piezoelectric energy harvesters applicable in factual wearables.

Broadband piezoelectric energy harvesting, wearable technology, DoE, frequency up-conversion, optimized geometry, experimental assessment

## 1. Energy harvesting in wearable technologies

Energy harvesting (EH) comprises the collection of low-level ambient energy and its conversion into usable electrical energy. Common energy forms suitable for EH are kinetic (vibrations, motion), thermal (waste heat), solar (photovoltaic) and radio frequency (RF), with kinetic energy, converted via the piezoelectric effect, being one of the most promising. The prevalent form of piezoelectric energy harvesters (PEHs) are bimorph cantilevers made up of two PZT layers on a metallic substrate (Fig. 1). The tip mass on the free end is used to tune the device to a specific excitation frequency, as well as to increase its deflection, and hence the resulting voltage [1].

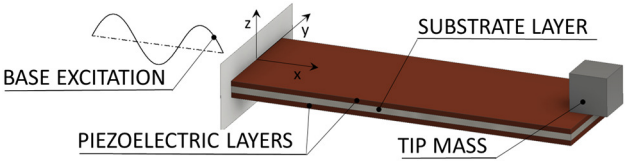


**Figure 1.** Bimorph piezoelectric energy harvester [2].

The rapid development of electronic devices, along with their ever-decreasing size and power requirements, brought along, in turn, new types of wearable devices. These require a power source, such as a battery, that can be efficiently replaced with an EH system. A new class of autonomous wearable devices, characterised by continuous operation, is hence enabled. Such devices can and are increasingly employed in medical, sports and work safety applications.

## 2. Energy from human motion and frequency up-conversion

Due to the random nature of human movements, there is no specific periodic excitation to which a wearable PEH can be tuned [3]. The energy conversion efficiency of a PEH rapidly decreases, however, when the excitation frequency moves away from its eigenfrequency. Converting random motion into periodical excitation by impacting or plucking the PEH free end (Fig. 2), and letting the bimorph oscillate at its eigenfrequency [4-6], i.e., employing what is generally referred to as "the frequency up-conversion (FUC) mechanism", provides a possible solution to this issue. The FUC effect can then be achieved by attaching one or several plectra to a flywheel, thus converting the random motion of the human body into a periodical plucking of PEH's free end via the plectra, hence exciting the oscillation of the PEH itself. This approach ensures that the PEH will always operate in its optimal working conditions, regardless of the random nature of the excitations, easing, therefore, the integration of EH technologies into wearable applications [2, 5].

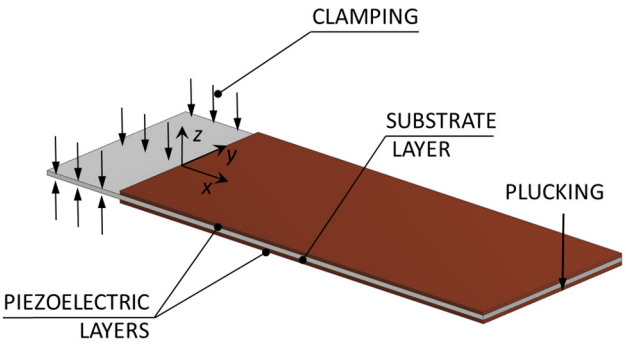


**Figure 2.** Frequency-up excitation of the PEH via periodic plucking.

## 3. Influence of the geometry on PEH's response

The typical shape of a PEH is a cantilever with a rectangular planar layout. By replacing this conventional shape with a trapezoid with an equal or comparable width, a significant increase in specific power output can be obtained. If the trapezoidal shape is inverted, i.e., clamped at the narrow end,

the specific power output can be increased even further [7]. Extensive finite element analyses (FEA) allow then evidencing that, when compared with a rectangular cantilever of the same overall surface area, a segmented solution with two trapezoids (A) and one inverted (B) PEH (Fig. 3a) allows obtaining a higher specific power output [4]. Such an approach enables, thus, a more efficient usage of the limited envelope of wearable devices, as well as a much simpler and, potentially, a more elegant solution for broadband PEHs. The addition of a triangular notch at the clamped end of a rectangular PEH (Fig. 3b), increases, in turn, cantilever's compliance and induces a boost in charge generation, resulting also in a marked increase of power output levels [4].

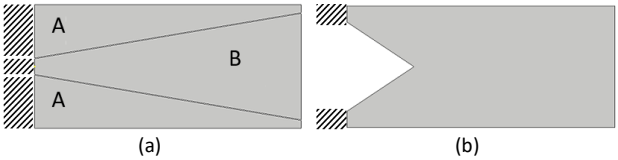


**Figure 3.** Segmented (a) and PEH with a triangular notch at the clamped end (b).

## 4. Geometry optimization and simulations

In all the performed analyses, the surface area of the considered PEHs is 15 x 23 mm, the thickness of the stainless steel substrate is 0.15 mm, the thickness of the parallelly connected PZT-5A active layers is 0.254 mm, with the resistive loads $R_L$ attached to the latter, while a 1g harmonic excitation is applied at the clamped end of the PEHs. To determine the ideal proportions of the segments and notches, i.e., those resulting in maximal power outputs, an optimization of their dimensions can be performed. In the case of the segmented shape, symmetry is used in this frame to reduce the time and resources required for the analyses, dividing hence the configuration into two equal parts and optimizing one half only. Two characteristic dimensions of the diagonal cut are thus considered (Fig. 4a). In the case of the notched shape, the width and the height of the notch are, in turn, optimised (Fig. 4b).

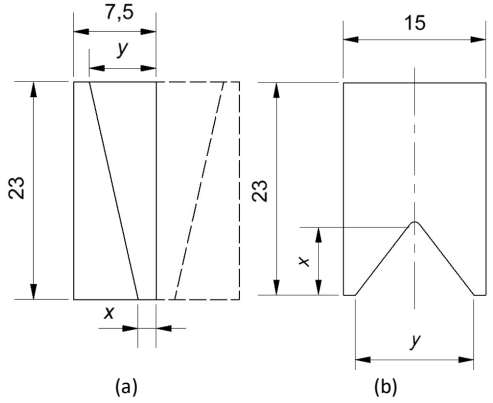


**Figure 4.** Optimisation parameters: segmented (a) and notched (b) PEH.

Using the central composite design-of-experiments (DOE) algorithm for two continuous factors, random combinations of the defining dimensions *x* and *y* are generated for each case [8]. The technological aspect is also considered, and the range of possible values of the dimensions is specified so as to allow enough space for the clamping and the tip mass attachments. A 3D FEA model is hence created for every combination of *x* and *y*, enabling to perform a number of modal and coupled harmonic analyses with varying load resistances. The maximum power output at an optimal load resistance is thus determined for each design configuration. The power output values are, then, paired with the respective characteristic dimensions, and the corresponding response surfaces are generated for each case, segmented and notched design configurations alike (Fig. 5 – the shown values for the segmented PEH are based on one half of the overall PEH). The respective regression equations are finally used to identify the combination of *x* and *y* values that result in the maximal power outputs.

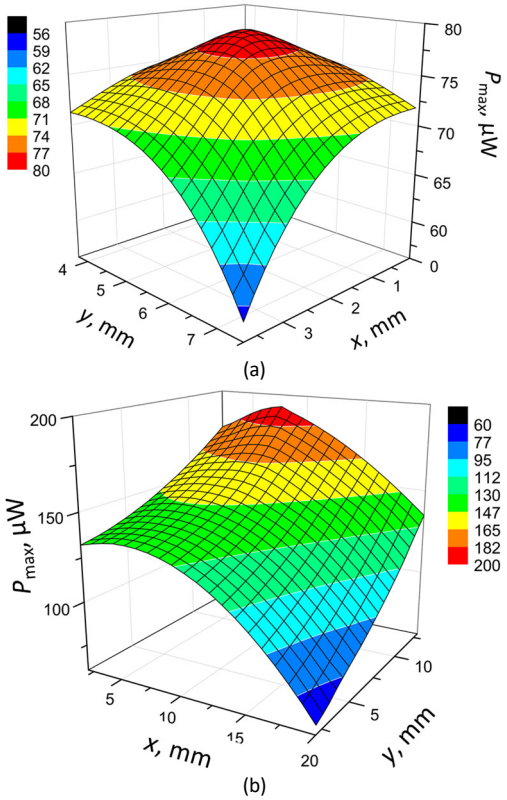


**Figure 5.** Response surfaces: segmented (a) and notched (b) PEH.

The optimal *x* and *y* values for the segmented and the notched PEHs are given in Table 1, along with the respective maximal power outputs and optimal load resistances obtained via coupled FEA (in this case the output powers for the trapezoidal segments comprise the sum for both of them).

**Table 1** Comparison of optimized PEH output parameters.

| | *x*/mm | *y*/mm | $R_L$/kΩ | $P_{max}$/µW | $P_{Smax}$/µW/m² |
|---|---|---|---|---|---|
| Trapezoidal | 1.5 | 7 | 7 | 26.3 | 175.5 |
| Inverted | | | 12 | 131.5 | 672.7 |
| Notched | 6.5 | 11 | 7 | 168.9 | 545.9 |
| Rectangular | - | - | 5 | 141.3 | 409.5 |

The graphical representation of the comparison of the respective trends is given in Fig. 6. As visible in Fig. 6a, the highest maximal output power ($P_{max}$) is obtained for the notched PEH. It can also be noted that the combined maximal power for the three segments of the segmented PEH also outperforms that of the conventional rectangular version. Since the basic configuration of the analysed bimorphs is kept constant in terms of the used materials and layer thickness, the specific power output ($P_{Smax}$), defined as the maximal power output divided by the surface of the respective geometry, can also be used as a suitable figure of merit. As shown in Fig. 6b, the highest specific power output is hence attained for the inverse trapezoidal segment. The second highest, still higher than that for the rectangular shape, is the specific power output of the notched shape. The specific power output of the two trapezoidal segments is, in turn, lower than that of the rectangular shape, but it should be perceived as an addition to the power generated via the inverse trapezoid.

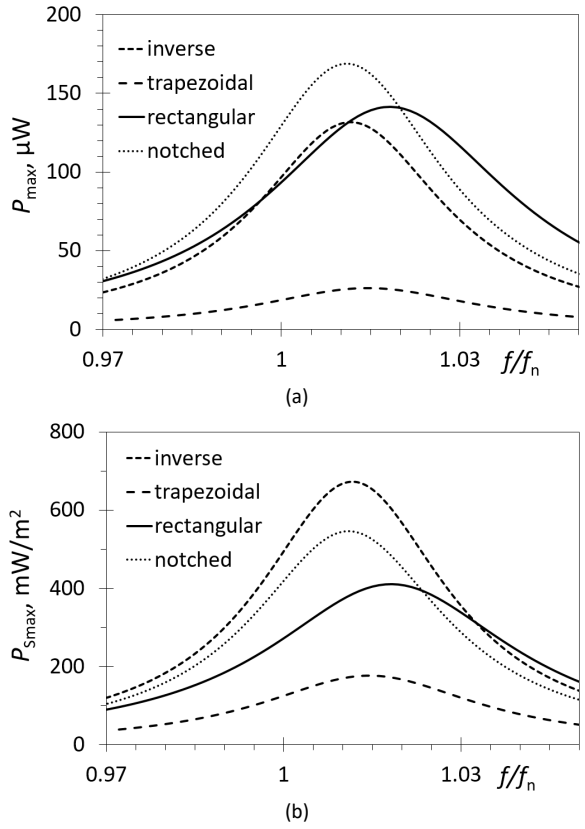


**Figure 6.** Power outputs for the segmented (a) and the notched (b) PEH.

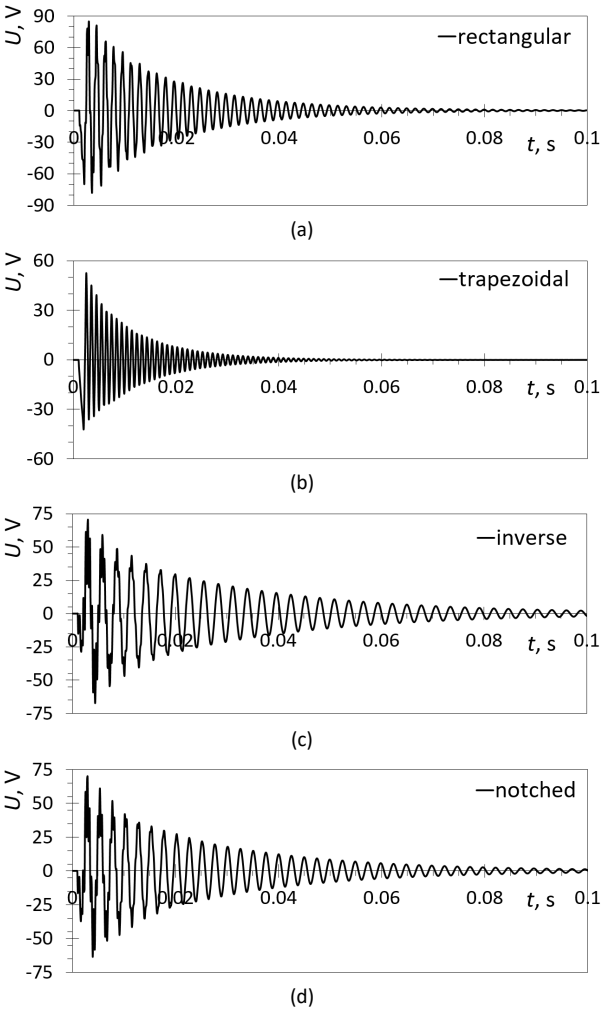


**Figure 7.** Voltage outputs for the plucked PEHs: rectangular (a), trapezoidal (b), inverse trapezoidal (c) and notched (d) PEH.

In addition to the modal and harmonic analyses, a transient coupled FEA of each optimized shape is performed as well, simulating the plucking of the free end of the PEHs. A comparison of the viability of the application of the FUC approach on optimized PEHs, with respect to the conventional rectangular configuration, can thus be appraised (Fig. 7). It can hence be observed that the maximum peak-to-peak voltage value of the inverse trapezoidal segment ($U_{p\text{-}p}$ = 137.6 V) is comparable to that of the conventional rectangular shape ($U_{p\text{-}p}$ = 161.5 V), even without considering the surplus voltage output from the two trapezoidal segments ($U_{p\text{-}p}$ = 94.3 V for each segment). The highest peak-to-peak voltage value for the triangular notched shape ($U_{p\text{-}p}$ = 133.3 V) is comparable to that of the inverse trapezoid, and thus a bit lower than that of the rectangular PEH. This proves, therefore, the feasibility of the application of the FUC approach for optimally segmented PEHs.

## 5. Experimental setups and preliminary results

In order to carry out the required harmonic and FUC measurements, two different experiments are developed. The harmonic analysis setup, shown in Fig. 8, comprises a Brüel&Kjær® LDS V201 electrodynamic permanent magnet shaker (1), powered via an LDS LPA100 power amplifier. The harmonic excitation is controlled via a NI LabVIEW® virtual instrument operating on an NI MyRIO 1900® device (2), which also serves as a DAQ system. The acceleration of the shaker is measured using a Vernier® 3D-BTA accelerometer (3), connected to a Vernier® BT-MDAQ adapter (4).

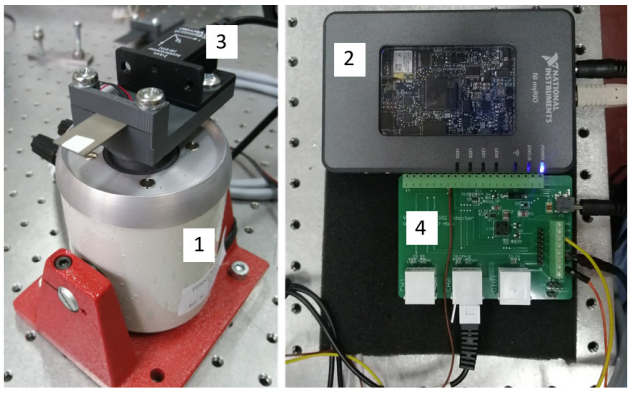


**Figure 8.** Experimental setup for harmonic analysis: B&K shaker with accelerometer (a), and respective control and DAQ components (b).

The FUC setup, shown in Fig. 9, comprises, on the other hand, a 3D printed excitation device made up by a clamping mechanism (1) and a DC motor with rotating interchangeable plectra (2). The power output is, in turn, measured by using an Agilent® DSO-X 2012A oscilloscope (3), while the displacement of the PEH free end is acquired by employing a Metrolaser® Vibromet 500V laser doppler vibrometer (4). To avoid the possible influence of magnets on the damping of the oscillating PEHs, a purely mechanical plucking is used here instead of the magnetic one [9].

A pure mechanical response of the analysed rectangular PEH is measured first. Based on this data, the logarithmic decrements $\delta$ and the damping ratio $\zeta$ are calculated. The damping ratio is, in fact, essential to calculate the Rayleigh damping coefficients $\alpha$ and $\beta$, utilized in FEA. The mechanical responses, measured by using the laser vibrometer, are thus generated by plucking the free end of the PEH, as well as by the base excitation via the shaker. A negligible difference is observed between the damping ratio values attained via the two different excitation methods, i.e., $\zeta$ = 0.03 in the case of the FUC, and $\zeta$ = 0.031 when the shaker base excitation is used (i.e., the difference is merely ~ 3 %).

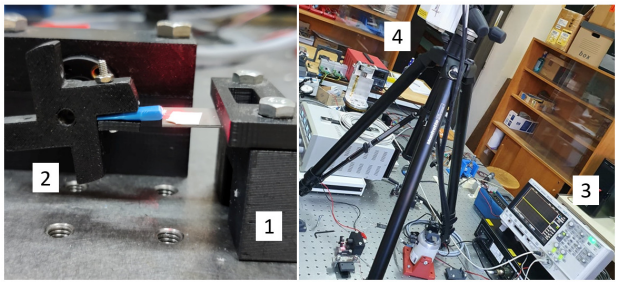


(a) (b)

**Figure 9.** FUC setup: plucking mechanism (a) and DAQ system (b).

To validate the developed numerical models, structured experimental campaigns, employing both the harmonic and the FUC setups, are performed next. Experimental data obtained via the harmonic excitation of the rectangular PEH, compared to the FEA results for the same geometry, are hence shown in Fig. 10. The boundary conditions used in the FEA model, i.e., the acceleration amplitude, the clamping condition and the used load resistances, are set to match as closely as possible those in the experimental setup. It is evident from the figure that the experimental results closely match those attained numerically. The experimentally accessed coupled eigenfrequency, as well as the maximum voltage, coincide with those attained via FEA ($U_{exp}$ = 4.02 V @ 552 Hz and $U_{FEA}$ = 4.03 V @ 555 Hz). There is, in turn, a slight dissimilarity in the overall width and shape of the two curves, which could perhaps be attributed to the still not completely accurate values of the Rayleigh damping coefficients used in the numerical model.

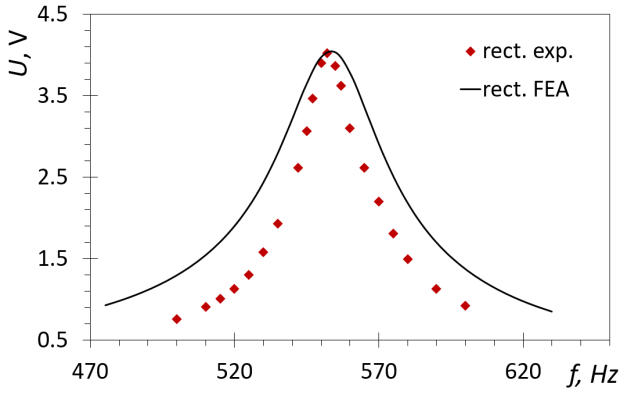


**Figure 10.** Comparison of experimental data and FEA results for a harmonically excited rectangular PEH.

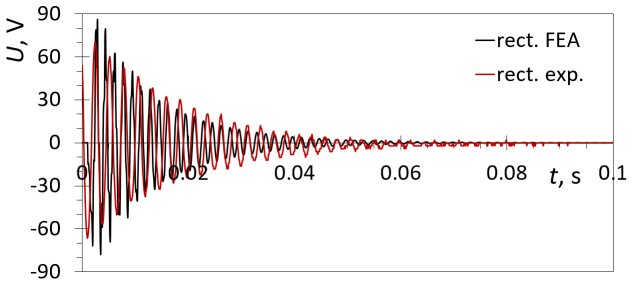


**Figure 11.** Experimental and FEA FUC responses for a rectangular PEH.

The experimental results for the rectangular PEH excited by plucking its free end (FUC), compared to the FEA results for the same geometry, are, in turn, shown in Fig. 11. The displacement of the plucked free end is set to 1 mm. It can thus be seen that there is a good match between the FEA and the experimental data. The maximum peak-to-peak voltage for the FE model is $U_{p\text{-}p\_FEA}$ = 162.5 V, while the experimentally attained voltage is $U_{p\text{-}p\_exp}$ = 142.6 V. The oscillation period in both cases is 0.08 s. The remining discrepancies are mainly due to plucking mechanism control, while those in the frequency can again be rectified by carefully tuning the FEA Rayleigh damping coefficients, as well as by devoting a meticulous attention to the clamping of the PEHs, since a very small difference in cantilever's length can have a noteworthy influence on PEHs' response.

## 6. Conclusions and outlook

Based on previous studies [2, 4], an optimization of two different PEH geometries is performed in this work based on the application of an advanced DOE approach. The optimal characteristic dimensions of two PEH design configurations are thus determined via a FEA approach, comprising modal, harmonic and transient analyses. The respective maximal and specific power outputs are hence obtained for the optimised PEHs and compared to those of a conventional rectangular PEH. It is thus established that the optimized shapes allow attaining significantly better performances both under harmonic and FUC excitations. Suitable experimental setups are therefore developed, and initial experiments are carried out, exhibiting a close match with numerical FEA data. The damping coefficient is also determined based on the experimental measurements.

Further experiments will be carried out next to assess the performances of optimised PEHs configurations determined in this work. What is more, a more detailed study is needed to understand better the effects of backward coupling and some of the damping effects. A careful approach to the clamping of the PEH base is also planned. A wearable prototype, based on flywheel driven plectra, converting random human motion into periodical excitation of the optimised PEHs, is also being developed to power an autonomous wearable device. This will finally comprise medical sensors (i.e., temperature, blood pressure or pulse monitoring), along with the appropriate communication components. The possibility of matching the power generated by each of the PEHs to different electrical load components, potentially resulting in an even more efficient system, will also be investigated in this frame. To enable a more efficient collection, conversion and storage of energy, a suitable power management system is also being developed and tested [2, 10]. In fact, research and optimisation of PEH-based integrated systems, especially those aimed at wearable applications, can lead to the development of a new type of autonomous wearable devices, with possible applications not only in remote patient monitoring, telemedicine, IoT and industry 4.0, but also, potentially, in aircraft structural health monitoring (SHM) systems [10].

## Acknowledgements

Work enabled by using the equipment funded via the EU ERDF project RC.2.2.06-0001 "Research Infrastructure for Campus-based Laboratories at the University of Rijeka – RISK", supported by the University of Rijeka grant uniri-tehnic-18-32 "Advanced mechatronics devices for smart technological solutions", and partially performed in the framework of the COST Action CA18203 "Optimizing Design for Inspection – ODIN".

## References

[1] Prya Sh and Inman D J 2009 *Energy harvesting technologies* (New York, NY, USA: Springer)
[2] Gljušćić P, Zelenika S et al. 2019 *Sensors* **19**(22) 4922
[3] Bai Y et al. 2018 *Mech. Syst. Signal Pr.* **106**:303-18
[4] Gljušćić P and Zelenika S 2020 *Proc. 20th EUSPEN Int. Conf.* 49-52
[5] Kuang Y and Zhu M 2017 *Sensor. Actuat. A* **263** 510-20
[6] Kathpalia B et al. A 2018 *Smart Mater. Struct.* **27**(1) 015024
[7] Benasciutti D et al. 2010 *Microsyst. Technol.* **16**(5) 657-68
[8] Dean A, Morris M, Stufken J and Bingham D (eds.) 2015 *Handbook of Design and Analysis of Experiments* (Boca Raton, FL, USA: CRC Press)
[9] Xue T et al. 2018 *Smart Mater. Struct.* **27**(8) 085026
[10] Zelenika S et al. 2020 *Sensors* **20** 6685